J Mol Model (2013) 19:1789–1799
DOI 10.1007/s00894-012-1730-7

ORIGINAL PAPER

DFT studies of the adsorption and dissociation of H_2O on the Al_{13} cluster: origins of this reactivity and the mechanism for H_2 release

Jian-Ying Zhao · Feng-Qi Zhao · Hong-Xu Gao · Xue-Hai Ju

Received: 25 September 2012 / Accepted: 10 December 2012 / Published online: 12 January 2013

Abstract A theoretical study of the chemisorption and dissociation pathways of water on the Al_{13} cluster was performed using the hybrid density functional B3LYP method with the 6-311+G(d, p) basis set. The activation energies, reaction enthalpies, and Gibbs free energy of activation for the reaction were determined. Calculations revealed that the H_2O molecule is easily adsorbed onto the Al_{13} surface, forming adlayers. The dissociation of the first H_2O molecule from the bimolecular H_2O structure via the Grotthuss mechanism is the most kinetically favorable among the five potential pathways for O–H bond breaking. The elimination of H_2 in the reaction of an H_2O molecule with a hydrogen atom on the Al cluster via the Eley–Rideal mechanism has a lower activation barrier than the elimination of H_2 in the reaction of two adsorbed H atoms or the reaction of OH and H. Following the adsorption and dissociation of H_2O, the structure of Al_{13} is distorted to varying degrees.

Keywords Al_{13} cluster · Water dissociation · Reaction mechanism · H_2 release · DFT

J.-Y. Zhao · X.-H. Ju (✉)
Key Laboratory of Soft Chemistry and Functional Materials of MOE, School of Chemical Engineering, Nanjing University of Science and Technology, Nanjing 210094, People's Republic of China
e-mail: xhju@mail.njust.edu.cn

J.-Y. Zhao
School of Chemistry and Chemical Engineering, Huaiyin Normal University, Huaian 223300, People's Republic of China

F.-Q. Zhao · H.-X. Gao
Laboratory of Science and Technology on Combustion and Explosion, Xi'an Modern Chemistry Research Institute, Xi'an 710065, People's Republic of China

Introduction

A blend of aluminum and water has been proposed as a propellant for use in both spacecraft and vehicles that travel underwater [1–3], because the combustion of Al_2O_3 is accompanied by the release of a large amount of heat. Scientists have performed a lot of studies on aspects of the characteristics of the combustion of aluminum with water, such as the effects of the size and shape of the aluminum particles on the combustion efficiency [4, 5] and the consequences of using aluminum alloys instead of pure aluminum [6–8]. Indeed, it has been noted that the chemical reactivity of the aluminum particles greatly depends on the size of the particles. For example, flame propagation speeds for metallic nanoparticles embedded in oxidizers are 0.9–1 km/s, as compared with 1–10 cm/s for micron-size particles [9]. This rapid nanoreaction cannot be explained by conventional mechanisms based on the mass diffusion of reactants, so various mechanisms for such enhanced nanoreactions have been proposed. Roach et al. [10, 11] experimentally studied reactions between heavy water (D_2O) and anionic Al_n clusters comprising 7–60 atoms, and proposed that introducing water onto Al_{16}^-, Al_{17}^-, and Al_{18}^- resulted in the production of H_2. Li et al. [12] investigated the interaction of an aluminum atom with a water molecule. Ab initio molecular dynamics simulations performed by Shimojo et al. [13, 14] indicated that hydrogen production is assisted by rapid proton transport in water via a chain of hydrogen-bond switching events similar to the Grotthuss mechanism (the usual mechanism by which protons tunnel from one water molecule to the next). These results are also in good agreement with those obtained from the DFT calculations performed by Flores et al. [15] on the interactions of individual Al atoms with water molecules. Flores [15] stated that the Al–H_2O interaction does not imply that a reaction occurs between these species, although experimental work [16, 17] indicated that there should

be a reaction that produces HAlOH. Michael et al. [18] investigated aluminum–water reactions using the ReaxFF reactive force field. They found that the dissociation of a water molecule assisted by unadsorbed H_2O is more energetically favorable.

To further elucidate the mechanism of the Al/H_2O reaction, we used the DFT-B3LYP method to investigate the interactions between H_2O and the Al_{13} cluster. This method has been widely used to study reaction pathways [19, 20]. We modeled the Al_{13} cluster for the following reasons. (1) The geometric structure of Al_{13} cluster is remarkably stable when compared with other aluminum clusters [21]. (2) The interactions of H_2O molecules with Al clusters are central to our understanding of the effects of cluster size on cluster behavior, and should provide useful insight into many real-world technological processes. (3) It will help to understand different mechanisms of water decomposition on the clusters rather than on the larger particles.

Computational details

All geometry optimizations were carried out using the the hybrid density functional B3LYP method with the 6-311+G (d, p) basis set. The B3LYP method has been found to give results similar to those yielded by the more computationally expensive MP2 theory for molecular geometry and frequency calculations, and gives good predictions of transition structure geometries [22, 23]. Different spin multiplicities of the Al_{13} were considered. Systems with doublet multiplicities for the reaction were chosen according to the results. Using the low-lying isomers of the Al_{13} cluster, we first considered H_2O at various initial adsorption sites on Al_{13}: a site atop an Al atom, a site bridging two Al atoms, and a hollow site (the center of a triangle Al face). The adsorption structures were then optimized without any symmetry constraints. Vibrational frequencies, the zero-point vibrational energy (ZPE), and thermodynamic contributions to the enthalpy and free energy of the reaction were calculated in order to find the minimum energy path (MEP) using intrinsic reaction coordinate (IRC) calculations [24, 25], to ensure that each transition state was linked to the desired reactant and product. It was confirmed that each calculated transition state had a single imaginary frequency, while each minimum only had real frequencies. All of the energies quoted and discussed in the present paper were corrected for ZPE. All calculations were performed with the GAUSSIAN 03 program package [26].

Figure 1 shows the low-energy configuration for the Al_{13} cluster. Nearest-neighbor Al–Al distances are in the range 2.650–3.017 Å, which is in good agreement with the range 2.63–3.01 Å previously reported by Wang [27] and the range 2.71–3.12 Å reported by Rao [28], and is comparable to the distances of 2.864 Å [29] and 2.618~2.958 Å [30] obtained experimentally for the bulk system. The optimized geometry for H_2O has bond lengths of 0.962 Å and a bond angle of 105.1°, consistent with the experimental values of 0.96 Å and 104.4°. These values indicate that the present set of exchange-correlation energy functionals is able to provide a good representation of the structural properties of the Al_{13} cluster and the isolated H_2O molecule. We therefore proceeded to investigate the adsorption of H_2O on the surface of Al_{13}.

The activation energy is defined as follows:

$$E_a = E_{TS} - \sum E_R, \quad (1)$$

where E_{TS} is the energy of the transition state and ΣE_R is the sum of the energies of the reactants.

Results and discussion

Adsorption and dissociation processes of H_2O

The reactions investigated in this work involve models I–V, as described below.

For Al_{13}+H_2O:

Model I:

$$Al_{13}+H_2O \xrightarrow{\text{Step 1}} Al_{13}H_2O \xrightarrow[\text{TS 1}]{\text{Step 2}} Al_{13}HOH$$

$$\xrightarrow[\text{TS 2}]{\text{Step 3}} Al_{13}O + H_2$$

$$\xrightarrow[\text{TS 3}]{\text{Step 4}} Al_{13}(H)_2O\text{-}1$$

For Al_{13}+$2H_2O$:

Model II:

$$Al_{13} + 2H_2O \xrightarrow{\text{Step 5}} o\text{-}Al_{13}(H_2O)_2 \xrightarrow[\text{TS 4}]{\text{Step 6}} Al_{13}HOHH_2O\text{-}1$$

$$\xrightarrow[\text{TS 5}]{\text{Step 7}} Al_{13}(OH)_2\text{-}1 + H_2 \xrightarrow[\text{TS 6}]{\text{Step8}} Al_{13}H(OH)O\text{-}1 + H_2$$

$$\xrightarrow[\text{TS 7}]{\text{Step 9}} Al_{13}O_2\text{-}1 + 2H_2$$

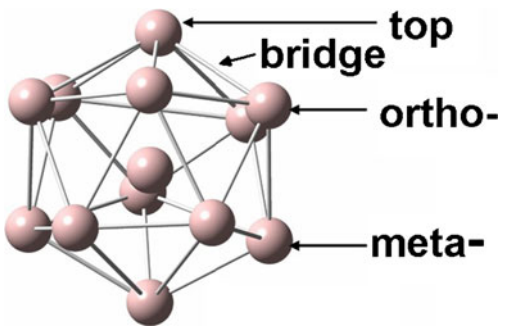

Fig. 1 The low-energy configuration of the optimized Al_{13} cluster

Model III:

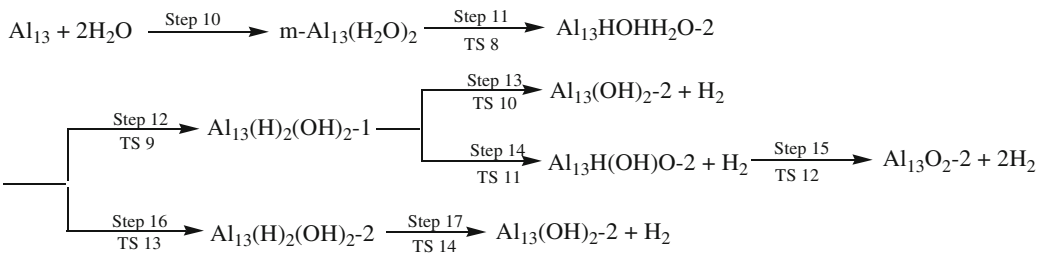

Model IV:

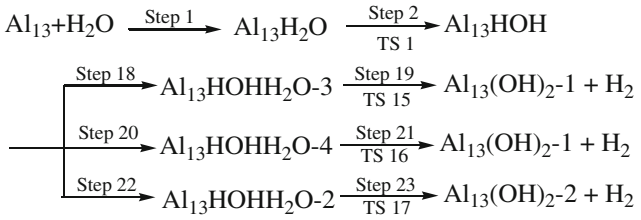

Model V:

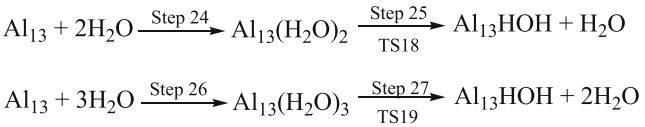

o-$Al_{13}(H_2O)_2$, *m*-$Al_{13}(H_2O)_2$, and $Al_{13}(H_2O)_2$ denote, respectively, an Al_{13} cluster with two H_2O molecules adsorbed "ortho" to each other (i.e., onto the two Al atoms on each side of an Al–Al bond), an Al_{13} cluster with two H_2O molecules adsorbed "meta" to each other (i.e., onto two Al atoms that are indirectly linked together by another Al atom), and an Al_{13} cluster with one H_2O molecule adsorbed onto the Al atom at the top of the cluster and the second H_2O molecule adsorbed on the first one (see Fig. 1).

In $Al_{13}(H_2O)_3$ (see Fig. 2), the second and third H_2O molecules are adsorbed onto the first one in a chain. In $Al_{13}(H)_2O$-1, the O atom bridges two adjacent Al atoms; one of these Al atoms has one of the H atoms on it, while the other H atom is meta to the O atom. In $Al_{13}HOHH_2O$-1, OH, H, and H_2O are adsorbed on three Al atoms that form a triangle on the surface of the cluster (i.e., OH, H, and H_2O are all ortho to each other). The OH is meta to the H_2O, whereas the H atom is ortho to the H_2O and meta to the OH group in $Al_{13}HOHH_2O$-2. An H_2O molecule forms a bridge between the OH group and the H atom in $Al_{13}HOHH_2O$-3. In $Al_{13}HOHH_2O$-4, H_2O is meta to OH and ortho to H, while OH is ortho to H (this structure was optimized from $Al_{13}HOH+H_2O$). $Al_{13}(OH)_2$−1 and $Al_{13}(OH)_2$−2 have two ortho OH groups and two meta OH groups, respectively. $Al_{13}H(OH)O$−1 has H and O atoms adsorbed at adjacent bridging sites, and the OH is adsorbed on the Al atom that connects those adjacent bridging sites. $Al_{13}H(OH)O$−2 has the OH meta to O (which forms a bridge between two Al atoms) and the H ortho to both. $Al_{13}(H)_2(OH)_2$−1 has two meta OH groups and two H atoms that are both ortho to each other and to one of the OH groups, but meta to the other OH group. In $Al_{13}(H)_2(OH)_2$−2, there are two meta OH groups, one H that is ortho and meta to the two OH groups, and another H that forms a bridge between the Al atoms at which the ortho OH group and H atom are adsorbed. $Al_{13}O_2$−1 and $Al_{13}O_2$−2 have two O atoms adsorbed at ortho and meta bridging sites, respectively.

The optimized geometries (with atomic labels) of the reactants, intermediates, transition states (TS), and products involved in the reaction of Al_{13} with H_2O are shown in Fig. 2. The total energies of all of the species involved in the MEPs of the reactions, along with the relative energies, are collected in Tables 1 and 2. The energy profiles for the stationary and the saddle points on the potential energy surface (PES) are shown in Figs. 3, 4, 5, 6, 7.

Model I

The H_2O molecule was initially placed in various locations about 3.5 Å from the Al_{13}. It was found that initial bridged and hollow configurations convert into a configuration with the water molecule at the top after geometric optimization, resulting in the formation of $Al_{13}H_2O$. These results indicated that the top adsorption process is an automatic process (it has a negative Gibbs free energy difference, see Table 2). This result is in accord with that reported in [31, 32]. In $Al_{13}H_2O$, the Al1–O bond length is 2.054 Å and the O–H bond length is 0.969 Å, which is only 0.007 Å longer than that in the gaseous H_2O molecule. H_2O and Al_{13} form an absorbed complex in which the lone pair of the oxygen atom interacts with the aluminum cluster [31]. The relative energy of $Al_{13}H_2O$ with respect to the reactants is −30.86 kJ·mol^{-1}, which agrees with the energies reported in [10] (−26.96 kJ·mol^{-1}) and [31] (−32.19 kJ·mol^{-1} for $Al_{13}H_2O$).

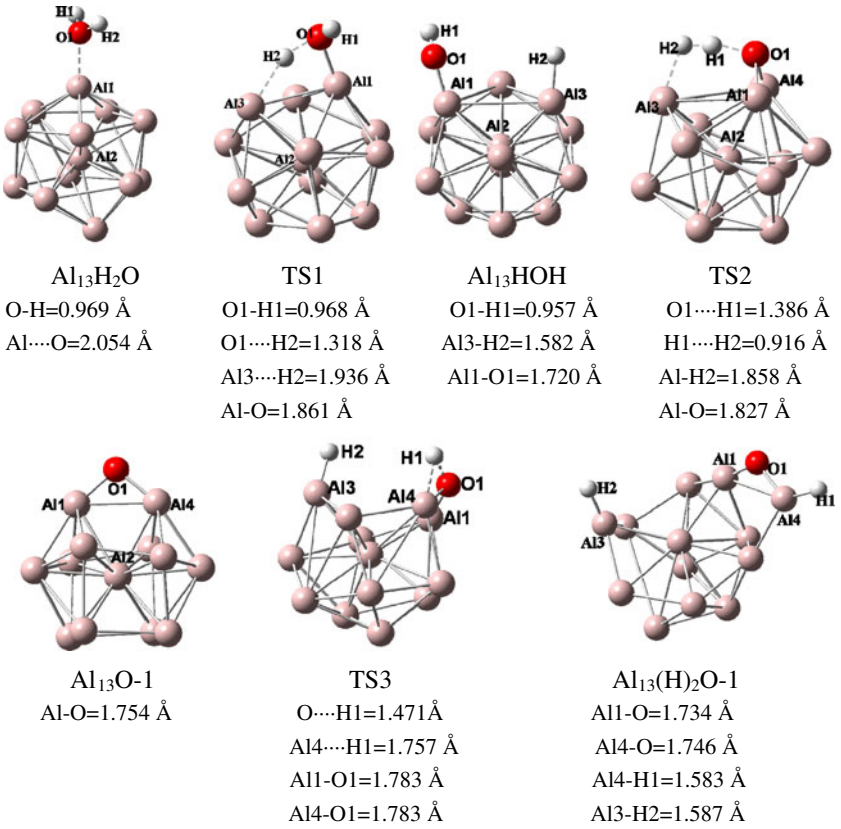

$Al_{13}H_2O$ TS1 $Al_{13}HOH$ TS2

$Al_{13}O$-1 TS3 $Al_{13}(H)_2O$-1

Fig. 2 Optimized geometries of the reactants, transition states (*TS*), and products on the PES associated with the reaction of Al_{13} with H_2O

After this initial absorption, the cluster undergoes O1–H2 bond dissociation. The O1–H2 bond stretches and the H2 transfers to an adjacent aluminum atom, forming $Al_{13}HOH$ through TS1. For $Al_{13}HOH$, there are possible two pathways to O1H1 group dissociation. In the first (step 3), ∠Al2–Al1–O1–H1 rotates with a rotational barrier of 0.18 $kJ \cdot mol^{-1}$ and points to H2. H1 then transfers from O1H1 to H2, eliminating H_2, and the O1 atom binds to the Al1 and Al4 atoms, forming $Al_{13}O$ via TS2. In the second dissociation pathway (step 4), H1 transfers from O1–H1 to its neighboring Al4 atom, forming an Al4–O bond and ultimately $Al_{13}(H)_2O$-1 via TS3.

Model II

According to this mechanistic hypothesis, two H_2O molecules were initially located about 3.5 Å atop two ortho Al atoms, but geometric optimization resulted in the formation of *o*-$Al_{13}(H_2O)_2$. There are then two possible pathways for H_2O decomposition on *o*-$Al_{13}(H_2O)_2$. One is via steps 6 and 7 to $Al_{13}(OH)_2-1$; the other is a direct process in which the two water molecules in contact in *o*-$Al_{13}(H_2O)_2$ react and form $Al_{13}(OH)_2-1$. However, a TS search failed to locate the latter pathway.

In step 6, the H2–O1 bond of the H1O1H2 molecule breaks and H2 binds to Al3, forming $Al_{13}HOHH_2O-1$ via TS4. In $Al_{13}HOHH_2O-1$, the distance O1–H4 is 1.676 Å and the angle O2–H4···O1 is 154.0°. The results indicate that O1 and H4 form a strong hydrogen bond. In step 7, the second H_2O is split into H4 and O2H3. At the same time, H2 ruptures from Al2–H2 and the hydrogen bond O1···H4 breaks. H4 and H2 combine via TS5, resulting in the elimination of an H_2 molecule and the formation of $Al_{13}(OH)_2-1$.

A further dehydrogenation reaction takes place in $Al_{13}(OH)_2-1$. In step 8, the O1H1 group shifts to the bridging site between Al1 and Al4 and forms two Al–O1 bonds. At the same time, the O1–H1 bond breaks and H1 moves into the bridging site between Al3 and Al4, forming $Al_{13}H(OH)O$. In the next step (step 9), the Al3–H1 bond in $Al_{13}H(OH)O$ ruptures and the O2H3 group shifts from the top of Al4 to the bridging site between Al3 and Al4, leading to the formation of two Al–O2 bonds. The ruptured H1 and H3 atoms bind with each other, forming H_2. After H_2 has been eliminated, $Al_{13}O_2-1$ is formed.

Model III

The suggested reaction processes here include steps 10–17. In step 10, two H_2O molecules are initially located about 3.5 Å atop of two adjacent Al atoms. The final state has two

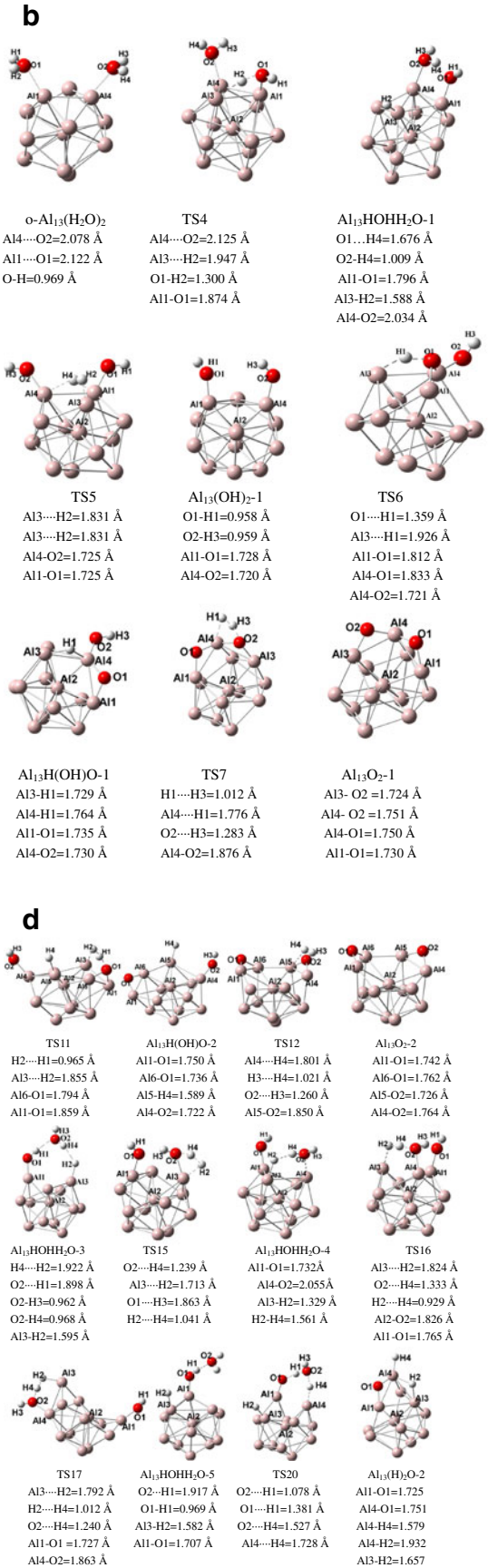

Fig. 2 (continued)

Table 1 Total energies (E_T), deformation energies (E_{def}), and number of imaginary frequencies (n_i) for the reactants, product complexes, and transition states on the PES

Species	E_T (Ha)	E_{def} (kJ·mol^{-1})	n_i
Al_{13}	−3151.968425	0.00	0
$Al_{13}H_2O$	−3228.417351	7.00	0
TS1	−3228.399853	9.37	1 (1449 cm^{-1}, i)
$Al_{13}HOH$	−3228.452165	25.00	0
TS2	−3228.417470	35.25	1 (1278 cm^{-1}, i)
$Al_{13}O$	−3227.284016	19.18	0
TS3	−3228.385827	8.72	1 (1122 cm^{-1}, i)
$Al_{13}(H)_2$−1	−3228.477648	179.21	0
o-$Al_{13}(H_2O)_2$	−3304.862701	11.28	0
TS4	−3304.844779	14.45	1 (1489 cm^{-1}, i)
$Al_{13}HOHH_2O$−1	−3304.912023	100.97	0
TS5	−3304.897137	33.56	1 (1150 cm^{-1}, i)
$Al_{13}(OH)_2$−1	−3303.755998	28.53	0
TS6	−3303.721216	58.42	1 (1592 cm^{-1}, i)
$Al_{13}H(OH)O$−1	−3303.781597	62363	0
TS7	−3303.753642	86.98	1 (1452 cm^{-1}, i)
$Al_{13}O_2$−1	−3302.61658	82.78	0
m-$Al_{13}(H_2O)_2$	−3304.860091	7.03	0
TS8	−3304.846285	18.87	1 (1506 cm^{-1}, i)
$Al_{13}HOHH_2O$−2	−3304.901589	48.71	0
TS9	−3304.887622	81.81	1 (1352 cm^{-1}, i)
$Al_{13}(H)_2(OH)_2$−1	−3304.941169	128.58	0
TS10	−3304.901918	58.58	1 (1524 cm^{-1}, i)
$Al_{13}(OH)_2$−2	−3303.754034	94.52	0
TS11	−3304.898359	126.29	−1223.4535
$Al_{13}H(OH)O$−2	−3303.781603	139.01	0
TS12	−3303.742912	61.91	1 (1520 cm^{-1}, i)
$Al_{13}O_2$−2	−3302.597625	46.72	0
TS13	−3304.874931	58.58	1 (1002 cm^{-1}, i)
$Al_{13}(H)_2(OH)_2$−2	−3304.938336	118.47	0
TS14	−3304.9024	97.21	1 (1219 cm^{-1}, i)
$Al_{13}HOHH_2O$−3	−3304.896686	29.56	0
TS15	−3304.878268	30.97	1 (1489 cm^{-1}, i)
$Al_{13}HOHH_2O$−4	−3304.89743	24.90	0
TS16	−3304.896682	28.04	1 (909. cm^{-1}, i)
TS17	−3304.880556	131.57	1 (1131 cm^{-1}, i)
$Al_{13}(H_2O)_2$	−3304.870241	7.53	0
TS18	−3304.861526	12.85	1 (1140 cm^{-1}, i)
$Al_{13}(H_2O)_3$	−3381.327268	7.92	0
TS19	−3381.304149	23.60	1 (990 cm^{-1}, i)
$Al_{13}HOHH_2O$−5	−3304.89467	27.27	0
TS20	−3304.828093	72.58	1 (918 cm^{-1}, i)
$Al_{13}(H)_2O$−2	−3228.511474	180.51	0

H_2O molecules adsorbed at the meta sites of Al_{13} after optimization.

In step 11, the H2 atom of the H1O1H2 molecule dissociates and bonds with Al3 to produce $Al_{13}HOHH_2O$–2 via TS8. In $Al_{13}HOHH_2O$–2, the geometry of the other H_2O (label: H3O2H4) barely changes.

The next dehydrogenation pathway also has three possible processes. First, in steps 12–13, the O2–H4 bond in the other H_2O dissociates and the H4 atom combines with the neighboring Al5 atom, which is located at the end of the bridge between Al3 and Al5, forming $Al_{13}(H)_2(OH)_2$−1 via TS9 (step 12). In the conversion from $Al_{13}(H)_2(OH)_2$−1 to $Al_{13}(OH)_2$−2 (step 13), H2 and H4 approach each other, and $Al_{13}(OH)_2$−2 is formed via TS10. Second, steps 12, 14, and 15 (similar to step 3) can take place via TS11 and TS12, with the formation of $Al_{13}O_2$−2. Finally, in steps 16–17, the O2–H4 bond of the other H_2O dissociates and the H4 atom combines with the bridging site between Al3 and Al4, forming $Al_{13}(H)_2(OH)_2$−2 via TS13 (step 16). In step 17, TS14, which links $Al_{13}(H)_2(OH)_2$−2 and $Al_{13}(OH)_2$−2, is only slightly different in terms of its geometry and energy from TS10 (the energy of TS10 is only 1.20 kJ·mol^{-1} higher than that of TS14).

Model IV

In this scenario, after one H_2O molecule has dissociated and $Al_{13}HOH$ has formed, another H_2O molecule is absorbed and then decomposes (Fig. 2). There are three possible pathways. In the first pathway (steps 18 and 19), the second H_2O (label: H3O2H4) molecule inserts between the O1H1 group and the H2 atom of $Al_{13}HOH$, forming $Al_{13}HOHH_2O$−3. In $Al_{13}HOHH_2O$−3, the distance O2−H1 is 1.898 Å. This shows that the H_2O molecule bonds with $Al_{13}HOH$ by a strong hydrogen bond. In the conversion from $Al_{13}HOHH_2O$−3 to $Al_{13}(OH)_2$−1, the H_2O molecule further inserts itself between OH and H2, breaking the hydrogen bond. H4 and H2 approach each other and the resulting H_2 is eliminated via TS15.

In the second pathway (steps 20 and 21), the second H_2O molecule is absorbed on Al4, which then forms a triangle with Al1 (which combines with the O1H1 group) and Al3 (which combines with H2), forming $Al_{13}HOHH_2O$−4. In $Al_{13}HOHH_2O$−4, the distance from H2 to H4 is 1.561 Å, which indicates that there is a rather weak interaction between H4 and H2. In the conversion from $Al_{13}HOHH_2O$−4 to $Al_{13}(OH)_2$−1, H2 and H4 move towards each other until H_2 forms and is eliminated via TS16.

In the third pathway (steps 22 and 23), the second H_2O molecule is absorbed on an Al atom, forming $Al_{13}HOHH_2O$ −2. A dehydrogenation reaction (step 23), similar to that of step 21, then occurs via TS17.

Model V

In this model, the dissociation of an H_2O molecule occurs between the water molecules, resulting in the formation of

Table 2 Free energies and entropies of activation and calculated rate constants (k), equilibrium constants (Keq) of the different steps (all of the energy values include the zero point correction)

Parameter	1	2	3	4	5	6	7	8	9	10	11	12	13	14	15
ΔS (cal·mol^{-1})	−26.57	−0.14	17.57	−10.48	−59.53	−9.67	36.20	−9.37	23.71	−60.5	−1.97	−0.01	25.08	19.52	20.82
ΔH (kJ·mol^{-1})	−31.88	−91.38	−0.76	−70.64	−55.41	−133.55	−26.53	−71.47	−6.62	−48.45	−109.57	−103.92	50.98	−4.82	21.95
ΔG (kJ·mol^{-1})	−23.96	−91.34	−6.00	−67.52	−37.67	−130.67	−37.32	−68.68	−13.69	−30.42	−108.98	−103.92	43.51	−10.63	15.74
K_{eq}	1.58×10^{4}	1.02×10^{16}	11.2	6.84×10^{11}	4.01×10^{6}	8.03×10^{22}	3.48×10^{6}	1.09×10^{12}	2.50×10^{2}	2.15×10^{5}	1.27×10^{19}	1.64×10^{18}	2.33×10^{-8}	7.30×10	1.74×10^{-3}
E_a (kJ·mol^{-1})		45.95	91.10	174.18		47.06	39.09	91.33	73.42		36.25	36.37	103.06	112.41	82.98
k (s^{-1})		6.75×10^{4}	1.07×10^{-3}	1.83×10^{-18}		5.34×10^{4}	6.16×10^{5}	1.03×10^{-3}	1.01		4.82×10^{6}	3.75×10^{6}	5.66	3.06×10^{-7}	3.84×10^{-2}

Parameter	16	17	18	19	20	21	22	23	24	25	26	27	28	29
ΔS (cal·mol^{-1})	−3.74	28.81	−34.00	27.71	−38.67	32.38	−35.77	25.08	−63.65	36.95	−93.42	66.71	−28.64	11.93
ΔH (kJ·mol^{-1})	−98.56	45.62	−22.31	−69.71	−25.35	−66.66	−34.53	−52.94	−77.28	−45.99	−131.82	8.56	−15.29	−59.80
ΔG (kJ·mol^{-1})	−97.45	37.03	−12.18	−77.97	−13.84	−76.31	−23.88	−60.41	−58.31	−56.99	−103.99	−11.32	−6.75	−63.35
K_{eq}	1.21×10^{17}	3.22×10^{-7}	1.36×10^{2}	4.64×10^{13}	2.66×10^{2}	2.38×10^{13}	1.53×10^{4}	3.88×10^{10}	1.66×10^{10}	9.77×10^{9}	1.68×10^{18}	9.64×10	2.69×10	1.27×10^{11}
E_a (kJ·mol^{-1})	69.99	94.42		48.36		1.96		55.23		22.88		60.71		174.80
k (s^{-1})	7.77×10^{-6}	1.89×10^{-4}		2.95×10^{4}		5.11×10^{12}		4.79×10^{4}		1.08×10^{9}		2.23×10^{2}		2.93×10^{-18}

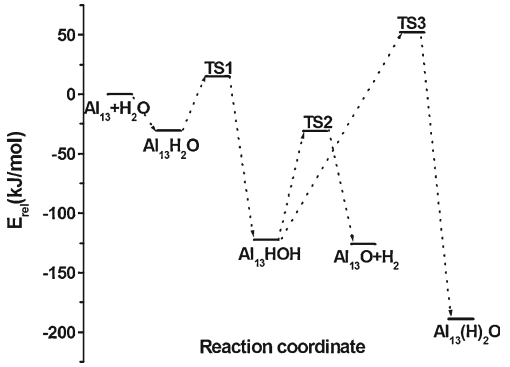

Fig. 3 Potential energy surfaces plotted against the reaction coordinate for steps 1–4, as calculated at the B3LYP/6-311+G(d,p) level

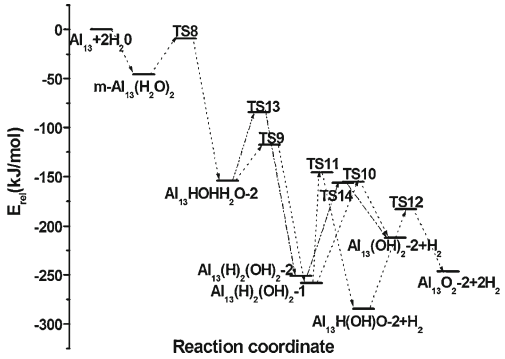

Fig. 5 Potential energy surfaces plotted against the reaction coordinate for steps 10–17, as calculated at the B3LYP/6-311+G(d,p) level

adlayers and Al_{13} (Fig. 2). In step 24, after an H_2O molecule has been absorbed, the second H_2O molecule combines with the first H_2O molecule by hydrogen bonding. The reaction begins with the dissociation of an H_2O molecule on an Al atom (step 25), and H2 moves toward the absorbed H_2O molecule to form a hydronium ion via TS18. Finally, a hydrogen in the hydronium ion bonds with the adjacent site of the adsorbed OH. This shows how the Grotthuss mechanism assists the decomposition of water molecules.

Steps 26 and 27 are similar to steps 24 and 25, respectively, with a total of three H_2O molecules involved. These three water molecules are adsorbed one by one via hydrogen bonding. H_2O is eliminated via TS19.

Reaction kinetics and thermodynamics of Al_{13} with H_2O

Table 2 lists values for the Gibbs free energy difference (ΔG) and other important thermodynamic and kinetic parameters of all the reaction steps at 298.15 K and 1 atm. The equilibrium constants for all of the reaction steps were calculated from the Gibbs free energies using $\Delta G=-RT\ln K_{eq}$.

Rate constants were determined using the generalized form of the Eyring equation [33–35]:

$$k = \frac{k_B T}{h} c_0^{1-m} e^{-\Delta G^{\#}/RT} \quad (3)$$

where m is the number of species that participate in the reaction, c_0 is the standard concentration, taken to be 1 mol/dm^3 (used to ensure that both sides of the equation have the same dimensions), k_B is the Boltzmann constant, T is the absolute temperature, and $\Delta G^{\#}$ is the free energy of activation. The calculated rate constants for all of the steps are also given in Table 2. The energy profiles are shown in Figs. 3, 4, 5, 6, and 7.

The calculated ΔH (298 K) for $Al_{13}+H_2O \rightarrow Al_{13}H_2O$ is -31.88 kJ·mol^{-1}, which is in good agreement with previously calculated values of -30.72 and -33.44 kJ·mol^{-1} for $Al+H_2O \rightarrow AlOH_2$ [10, 36]. This result shows that the computational method employed in this work is able to provide a good representation of the thermodynamic properties of the reaction of Al_{13} with H_2O.

Judging by the values of ΔG and K_{eq} for steps 1, 5, 10, 18, 20, 22, 24, and 26, H_2O molecules are easily adsorbed onto the surface of Al_{13}. The ΔG values of o-$Al_{13}(H_2O)_2$ and m-$Al_{13}(H_2O)_2$ with respect to that of ($Al_{13}H_2O+H_2O$) are -13.70 kJ·mol^{-1} and -6.51 kJ·mol^{-1}, respectively. The

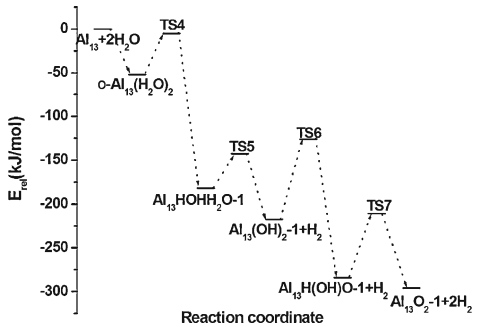

Fig. 4 Potential energy surface plotted against the reaction coordinate for steps 5–9, as calculated at the B3LYP/6-311+G(d,p) level

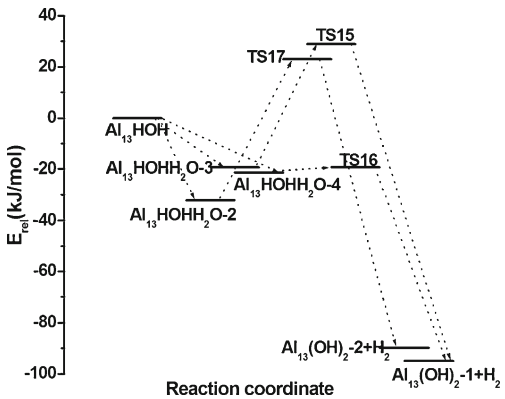

Fig. 6 Potential energy surfaces plotted against the reaction coordinate for steps 18–23, as calculated at the B3LYP/6-311+G(d,p) level

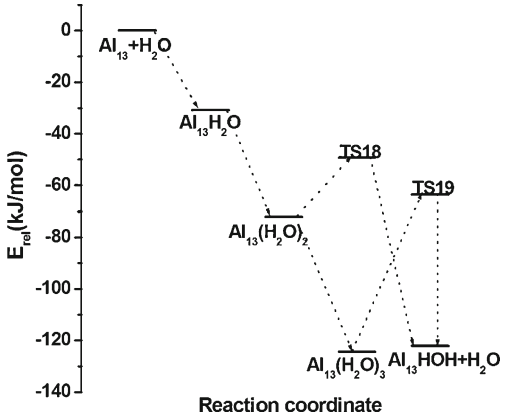

Fig. 7 Potential energy surfaces plotted against the reaction coordinate for steps 24–27, as calculated at the B3LYP/6-311+G(d,p) level

ΔG between $Al_{13}(H_2O)_2$ and ($Al_{13}H_2O$+H_2O) is −34.35 kJ·mol^{-1}, and it is −45.68 kJ·mol^{-1} between $Al_{13}(H_2O)_3$ and ($Al_{13}(H_2O)_2$+H_2O). These results show that the formation of H_2O molecular adlayers is thermodynamically favorable.

There are five possible pathways (steps 2, 6, 11, 25, and 27) for the dissociation of the first water molecule. Table 2 shows that they all have large K_{ep} values and low energy barriers except for step 27. Steps 2, 6, and 11 represent the dissociation of water on the surface of Al_{13} with energy barriers of 45.95, 47.06, and 36.25 kJ·mol^{-1}, respectively. The corresponding dissociation rates are k=10^4–10^6 s^{-1}. In steps 25 and 27, one of the hydrogen atoms from an adsorbed water molecule is removed by a solvated water molecule. The activation energy for step 25 (22.88 kJ·mol^{-1}), which is in line with a previous result (19.30 kJ·mol^{-1} [11]), is the smallest, and its k value (10^9 s^{-1}) is the largest among all five steps. In [16], it was found that the dissociation of an isolated water molecule on the Al surface requires significant activation energy, and that an assisted dissociation process involving a neighboring unadsorbed water molecule is more energetically favorable. Our calculated results are in agreement with those reported in [16]. This also shows that the Grotthuss mechanism greatly reduces the activation barrier for the dissociation. The energy barrier of step 27 (60.71 kJ·mol^{-1}), which also represents the Grotthuss mechanism, is larger than that of step 25. This is identical to the results reported in [11]. Shimojo et al. indicated that the large E_a of step 27 is caused a chained complex consisted of three water molecules onto the Al cluster [11].

There are two ways for the second H_2O molecule to dissociate after the first H_2O molecule has done so. In step 12, the k and ΔG values of the dissociation reaction are as large as those in step 11. These show that the products of the dissociation of the first H_2O molecule do not significantly affect the dissociation of the second H_2O molecule. This could be because the H and the OH group are adsorbed onto different Al atoms. Step 16 is energetically favorable but kinetically unfavorable due to the repulsion between the first adsorbed H atom (H2) and the second adsorbed H atom (H4) on Al3.

There are three possible paths to H_2 elimination. One pathway (steps 7, 19, 21, or 23) involves an H_2O and an adsorbed H atom. Step 7 ($Al_{13}HOHH_2O$−1 → $Al_{13}(OH)_2$−1), step 21 ($Al_{13}HOHH_2O$−4 → $Al_{13}(OH)_2$−1), and step 23 ($Al_{13}HOHH_2O$−2 → $Al_{13}(OH)_2$−1) involve the Eley–Rideal mechanism. In this mechanism, one H_2O molecule that is only weakly adsorbed on the surface collides with a chemisorbed H on the surface. The energy of $Al_{13}HOHH_2O$−1 is lower than that of $Al_{13}HOHH_2O$−4, as shown in Table 1. The adsorbed H_2O molecule and OH group are linked by a hydrogen bond in the configuration $Al_{13}HOHH_2O$−1. Therefore, it is more difficult to eliminate H_2 from $Al_{13}HOHH_2O$−1 (step 7) than from $Al_{13}HOHH_2O$−4 (step 21). In steps 21 and 23, the energy of $Al_{13}HOHH_2O$−4 is larger than that of $Al_{13}HOHH_2O$−2, while the energies of TS16 and $Al_{13}(OH)_2$−1 are lower than those of TS17 and $Al_{13}(OH)_2$−2, respectively. Therefore, step 21 is the most kinetically favorable of these steps. Step 19 is similar to the Grotthuss mechanism. For steps 7, 21, 23, and 19, all of the ΔG values are negative, and the corresponding rate constants are k=6×10^5, 5×10^{12}, 5×10^4, and 3×10^4 s^{-1}, respectively. The other two pathways for H_2 elimination (steps 3, 9, 14, and 15, and steps 13 and 17, respectively) involve an interaction between an adsorbed OH and an H atom, and an interaction between an adsorbed H and another H atom, respectively. These steps can be classified as Langmuir–Hinshelwood mechanisms. The energy barriers for steps 13 and 17 are 103.06 kJ·mol^{-1} (1.07 eV) and 94.42 kJ·mol^{-1} (0.98 eV), respectively. As shown in Table 2 and Figs. 3, 4, 5, 6, and 7, the rates of these steps range from 2×10^{-4} to 6 s^{-1}. These results show that the latter two pathways are less kinetically favorable than the first pathway, which is in accord with previously calculated results [11].

Judging by the ΔG and k values of steps 4 and 8, both of these steps (dissociation of the OH group adsorbed on the Al surface) are exothermic but have large energy barriers. We investigated this dissociation by adsorbing an H_2O molecule onto OH (see Table 2, steps 28 and 29) or by inserting the water molecule between two adsorbed OH groups. The results indicate that these steps are kinetically unfavorable.

After adsorbing and dissociating water, the structure of the Al_{13} cluster is distorted. The calculated deformation energies (E_{def}) of Al_{13} are also listed in Table 1. It is clear that, on the whole, the larger the adsorption energy or reaction energy, the larger the deformation energy.

Conclusions

The mechanism of the reaction between the Al_{13} cluster and water in the gas phase has been investigated using a DFT method. Five models of the adsorption and dissociation of water on the Al_{13} cluster were considered. Calculations reveal that it is more energetically favorable for water molecules to form adlayers on Al_{13}. All steps in the dissociation of the first H_2O molecule, forming OH and H, are energetically and kinetically favorable. However, dissociation from the bimolecular H_2O structure via the Grotthuss mechanism is the most kinetically favorable. This indicates that the dissociation rate of water is related to its initial concentration: too few water molecules lead to 100 % adsorption, so there are no unabsorbed molecules left to assist with the dissociation, whereas too many water molecules leads to the formation of multilayers on the Al_{13}, which reduces the dissociation rate. A hydrogen molecule is produced from the water molecule and the hydrogen atom adsorbed on the Al cluster; this pathway has a lower activation barrier than that involving the reaction of two adsorbed hydrogen atoms or that in which a hydrogen atom and an OH group are adsorbed. This shows that the production of a hydrogen molecule via the Eley–Rideal mechanism is more favorable than its production via the Langmuir–Hinshelwood mechanism. The direct dissociation of the adsorbed OH group on the surface of the Al_{13} cluster is exothermic but has a large energy barrier. After adsorbing and dissociating H_2O, the structural symmetry of the Al_{13} cluster is destroyed, leading to varying degrees of distortion.

Acknowledgments The authors gratefully acknowledge the funding provided by the Laboratory of Science and Technology on Combustion and Explosion (grant no. 9140C35010201) for this work. J.Y.Z. thanks the Innovation Project for Postgraduates in Universities of Jiangsu Province (grant no. CXLX11_0246) for partial financial support.

References

1. Bruno C, Ingenito A, Cuoco F (2002) Using powdered aluminum for space propulsion. In: Proc 18th Int Workshop on Rocket Propulsion: Present and Future, Pozzuoli, Italy, 16–20 June 2002, pp 16–20
2. Miller TF, Herr JD (2004) Green rocket propulsion by reaction of Al and Mg powders and water. In: 40th AIAA/ASME/SAE/ASEE Joint Propulsion Conf and Exhibition, Fort Lauderdale, FL, USA, 11–14 July 2004, paper 2004-4037
3. Ingenito A, Bruno C (2004) Using aluminum for space propulsion. J Propuls Power 20:1056–1063
4. Risha GA, Son SF, Yetter RA, Yang V, Tappan BC (2007) Combustion of nano-aluminum and liquid water. Proc Combust Inst 31:2029–2036
5. Deng ZY, Zhu LL, Tang YB (2010) Role of particle sizes in hydrogen generation by the reaction of Al with water. J Am Ceram Soc 93:2998–3001
6. Muntyana SP, Volodinab GF, Grabkob DZ, Zhitar VF (2009) An aluminum alloy for generation of hydrogen from water. Surf Eng Appl Electrochem 45:347–351
7. Diwan M, Hanna D, Shafirovich E, Varma A (2010) Combustion wave propagation in magnesium/water mixtures: experiments and model. Chem Eng Sci 65:80–87
8. Kozin LF, Volkov SV, Goncharenko SG, Permyakov VV, Danil'tsev BI (2011) Kinetics and mechanism of interaction of aluminum and magnesium of Al–Mg–Bi ternary system with water. Prot Met Phys Chem Surf 47:171–180
9. Levitas VI, Asay BW, Son SF, Pantoya M (2006) Melt dispersion mechanism for fast reaction of nanothermites. Appl Phys Lett 89:071909
10. Roach PJ, Woodward WH, Castleman AW Jr, Reber AC, Khanna SN (2009) Complementary active sites cause size-selective reactivity of aluminum cluster anions with water. Science 23:492–495
11. Reber AC, Khanna SN, Roach PJ, Woodward WH, Castleman AW Jr (2010) Reactivity of aluminum cluster anions with water: origins of reactivity and mechanisms for H_2 release. J Phys Chem A 114:6071–6081
12. Sun YL, Tian Y, Li SF (2008) Theoretical study on reaction mechanism of aluminum-water system. Chin J Chem Phys 21:245–249
13. Ohmura S, Shimojo F, Kalia RK, Kunaseth M, Nakano A, Vashishta P (2011) Reaction of aluminum clusters with water J. Chem Phys 134:244702
14. Shimojo F, Ohmura S, Kalia RK, Nakano A, Vashishta P (2010) Molecular dynamics simulations of rapid hydrogen production from water using aluminum clusters as catalyzers. Phys Rev Lett 104:126102
15. Álvarez-Barcia S, Flores JR (2009) The interaction of Al atoms with water molecules: a theoretical study. J Chem Phys 131:174307
16. Oblath SB, Gole JL (1979) Aluminum hydration in the vapor-phase. J Chem Phys 70:581–582
17. Kauffman JW, Hauge RH, Margrave JL (1980) Infrared matrix-isolation studies of the interactions and reactions of group IIIA metal atoms with water. J Am Chem Soc 102:6005–6011
18. Russo MF Jr, Li R, Mench M, Duin ACT (2011) Molecular dynamic simulation of aluminum-water reactions using the ReaxFF reactive force field. Int J Hydrog Energy 36:5828–5835
19. Wójcik A, Borowski T, Broclawik E (2011) The mechanism of the reaction of intradiol dioxygenase with hydroperoxy probe A DFT study. Catal Today 169:207–216
20. Hadebe SW, Kruger HG, Robinson RS (2011) A DFT study of the hydroboration reaction with oxygen-, sulphur-, and nitrogen-based boranes. Comput Theor Chem 968:26–30
21. Zhang ZG, Xu HG, Feng Y, Zheng WJ (2010) Investigation of the superatomic character of Al_{13} via its interaction with sulfur atoms. J Chem Phys 132:161103
22. Tiwary AS, Mukherjee AK (2009) Mechanism of the CH_3NH_2–HNO_2 reaction: ab initio DFT/TST study. J Mol Struct (THEOCHEM) 909:57–65
23. Meyer MP, Delmonte AJ, Singleton DA (1999) Reinvestigation of the isotope effects for the Claisen and aromatic Claisen rearrangements: the nature of the Claisen transition states. J Am Chem Soc 121:10865–10874
24. Ishida K, Morokuma K, Komornicki A (1977) The intrinsic reaction coordinate. An ab initio calculation for HNC to HCN and H^-+CH_4 to CH_4+H^-. J Chem Phys 66:2153–2156
25. Gonzalez C, Schlegel HB (1990) Reaction path following in mass-weighted internal coordinates. J Phys Chem 94:5523–5527
26. Frisch MJ, Trucks GW, Schlegel HB, Scuseria GE, Robb MA et al (2003) Gaussian 03, revision C.02. Gaussian, Inc., Wallingford
27. Wang LG, Kuklja MM (2010) First-principles study of small aluminum clusters: oxygen adsorptions, oxidation and phase stability. J Phys Chem Solid 71:140–144

28. Rao BK, Jena P (1999) Evolution of the electronic structure and properties of neutral and charged aluminum clusters: a comprehensive analysis. J Chem Phys 111:1890
29. Cooper AS (1962) Precise lattice constants of germanium, aluminum, gallium arsenide, uranium, sulphur, quartz and sapphire. Acta Cryst 15:578–582
30. Tougait O, Noel H (2004) Stoichiometry of UAl_4. Intermetallics 12:219–223
31. Jin S, Head JD (1994) Theoretical investigation of molecular water adsorption on the Al(111) surface. Surf Sci 318:204–216
32. Calvin MD, Head JD (1996) Theoretically modelling the water bilayer on the Al(111) surface using cluster calculations. Surf Sci 345:161–172
33. Evans MG, Polanyi M (1935) Some applications of the transition state method to the calculation of reaction velocities, especially in solution. Trans Faraday Soc 31:875–894
34. Winzor DJ, Jackson CM (2006) Interpretation of the temperature dependence of equilibrium and rate constants. J Mol Recognit 193:89–407
35. Laidler KJ, King MC (1983) The development of transition-state theory. J Phys Chem 87:2657–2664
36. Sakai S (1992) Characterization of aluminum atom insertion mechanisms into fluorine–hydrogen, oxygen–hydrogen, nitrogen–hydrogen, chlorine–hydrogen, sulfur–hydrogen and phosphorus–hydrogen bonds by ab initio MO methods. J Phys Chem 96:8369–8373